Making, Breaking, and Shaping Contacts by Controlling Double Layer Forces

Joelle Frechette*,† and T. Kyle Vanderlick‡

Chemical and Biomolecular Engineering Department, Johns Hopkins University, Baltimore, Maryland 21218 and Chemical Engineering Department, Yale University, New Haven, Connecticut 06520

The development and understanding of electrostatic actuations in liquid solution can be a difficult task. The large voltages that are commonly employed for electrostatic actuation in air can cause electrolysis at the various solid−liquid interfaces. At the nanoscale, this challenge is compounded by the presence of various surface forces. We demonstrate that the electrochemical Surface Force Apparatus can be employed to characterize the response of electrostatic actuators in nanoscale gaps. We show that low voltage DC actuation can be used to cause displacements at the nanoscale due to variations in the electrical double layer. We also demonstrate that double layer forces can be used to make or break contact between two surfaces and even to cause surface deformations, all without mechanically moving either substrate. Control over displacement, and associated deformations, is obtained by varying the surface energy as accomplished by regulating the surface charge density. The displacement can be evaluated as a function of applied potential with subnanometer resolution.

Introduction

An ambitious goal for microelectromechanical systems (MEMS) is their operation in fluids for biological applications (Bio-MEMS).[1] However, certain aspects of MEMS devices need to be adapted for operation in fluids. For example, strategies to prevent unwanted adhesion (or stiction) need to be adapted for operation in solution,[2] and complications due to electrical double layers and ions in solutions force electrostatic actuators to operate with high frequency AC drive signals.[3] Even with these limitations, electrostatic actuation is a particularly attractive option in liquids, especially because of the increased range of motion of the actuator caused by the high dielectric constant of water (as compared to air or vacuum). Complexity is added to the design of an electrostatic actuator if it has to operate at the nanoscale and in liquids. When the gap between the actuator plates is between 10−100 nm the nature of the surfaces becomes increasingly important. Double layers forces, van der Waals interactions, and adsorption (or fouling) are present; and all of these factors can affect the response of a nanoscale actuator.

Voltage-displacement relationships are commonly employed to describe the behavior of electrostatic actuators and depend on the type and geometry of the actuator. For a parallel-plate electrostatic DC actuator (such as the one shown in Figure 1d), the capacitive force (F_{elec}) is balanced by the spring restoring force ($F_{mech} = kx$, where x is the displacement and k is the spring constant) and is proportional to the square of the applied voltage ($F_{elec} \alpha V^2$). For actuation in fluids, Sounart et al.[3] showed that the voltage-distance relationship depends on the drive frequency and is proportional to V^2 only above a critical frequency (for salt solution this frequency is in the MHz range).

The "pull-in" instability is another important characteristic of a parallel-plate electrostatic actuator. The pull-in instability is a spring instability that occurs during actuation when the gradient of the capacitive force (dF_{elec}/dx) is greater than the spring constant. Consequences of the pull-in instability are that (1) any separation beyond that of the onset of the pull-in instability is inaccessible via electrostatic actuation and (2) in the presence of surface forces (capillary, van der Waals, etc.) the mechanical restoring force of the actuator will not let the plate return to its original position once the applied voltage is removed. Typically, for a parallel-plate actuator, the onset of the pull-in instability occurs for separations less than 2/3 of the original gap between the plates, any larger displacement brings the plates in contact.[4−7] To determine the pull-in instability for actuation in liquid solutions, one must take into account the surface properties, the nature of the dielectric (both that of the insulating layer on the actuator and that of the fluid), and the stiffness of the spring. Rollier et al.[8] demonstrated that the

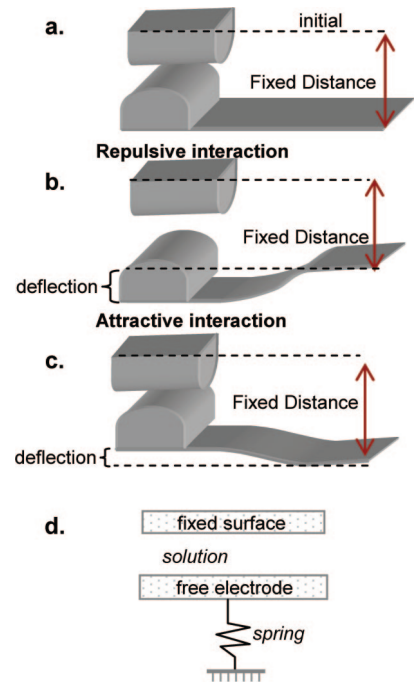

Figure 1. (a−c) Schematic of the approach described in this work. (a) Initially, the surfaces are brought close to contact (or in contact) using the microstepping motors. When the electrode potential is changed, the force between the two surfaces changes, which causes the cantilever spring to deflect. The measured change in surface separation is caused by the spring deflection and not an overall displacement (the motors are not used, i.e., the base of the spring does not move). The deflection for attractive (b) and repulsive (c) forces is shown. Part d shows the model of a typical electrostatic actuator.

* To whom correspondence should be addressed. E-mail: jfrechette@jhu.edu.
† Chemical and Biomolecular Engineering Department, Johns Hopkins University.
‡ Chemical Engineering Department, Yale University.

10.1021/ie800734y CCC: $40.75
Published on Web 08/29/2008

pull-in instability can be suppressed for an electrostatic actuator operating in liquids. Their experiments and analysis show that a larger range of motion can be achieved due to the dual effects of the insulating layer on the electrode (Si_xN_y) and the increase dielectric constant of the fluids. Their work involved microscale gaps and neglected potential charging effects and nonlinearities caused by the electrical double layer, which are present at the nanoscale.

As device designs are getting smaller, short-range effects such as van der Waals and double layer forces will become important and should be incorporated in the design of actuators. Recently, the work of Boyd and Kim[9] investigated the onset of the pull-in instability for electrostatic actuators in nanoscale gaps. Using the linearized Poisson−Boltzmann equation to calculate the electrostatic forces and a Hamaker constant approach to evaluate the van der Waals forces, they predicted important deviations from microscale voltage-displacement relationships and from the separation for the onset of the pull-in instability.

Due to the predominance of surface forces, the understanding and evaluation of nanoscale actuators lies at the heart of colloids and interfacial science. The AFM can be employed to determine force−distance relationships under various conditions (salt concentration, applied potentials, and surface chemistry)[10−13] and these results can be employed to refine the models for electrostatic actuation. Here, we show that the addition of external potential control with the surface forces apparatus (SFA) can be employed for a direct determination of the voltage-distance relationship in nanoscale gaps and direct investigation of the pull-in instability. We use the simple system of mica separated from potential-controlled gold as a testbed for study. The new type of measurements conducted with the SFA reported herein can allow for a systematic investigation of electrostatic actuation in nanogaps.

Experimental Section

Electrochemical SFA. The Electrochemical SFA is a modified version of the original SFA allowing potential control of one or both of the surfaces studied. The detailed experimental setup of the ESFA has been described previously[14−16] and only the salient points important to the understanding of this work will be detailed here. The two interacting surfaces discussed here are a gold electrode (specifically designed for the ESFA) and a cleaved mica surface. The surfaces are glued (Epon 1004) onto cylindrical supports ($R \approx 1-2$ cm) and oriented in a cross-cylindrical fashion. Due mainly to the compliance of the glue, the interacting "bodies" are readily deformable and the associated deformation is easily distinguished with multiple beam interferometry. The gold electrode is part of a three-electrode arrangement with the applied potential measured with respect to a Ag/Ag_2S wire.[17] The potential of the gold electrode is kept within the polarizable region throughout the experiment (i.e., there is no significant faradaic reaction occurring at the gold/solution interface). The measured potential is then translated to an Ag/AgCl(3M) scale by measuring the open circuit potential difference between the Ag/Ag_2S and the Ag/AgCl(3M) at the conclusion of the experiment. All applied potentials in this work are expressed with respect to the Ag/AgCl(3M) reference electrode.

Materials. Solutions of 1 mM $KClO_4$ with 1 mM pyridine were prepared from highest available purity solutes (Aldrich) which were used without further purification and dissolved in 18.2 MΩ deionized water (Hydro Services). The solutions were unbuffered and had a pH of about 5.5. The gold working electrode was made by thermal evaporation (ca. 2.0 Å/s) using high purity gold (99.999%, Cerac) and titanium (99.99%, Alfa). Solder was high purity indium (99.999%, Cerac) and covered with epoxy (Hysol 0151, Dexter). Mica sheets (Ruby, ASTM V-2, S&J Trading) were cleaved in a laminar hood and put on a larger mica backing sheet. This backing sheet was then coated with a silver film (99.999%, Alfa) approximately 48-nm thick (formed at a rate of 3.5 Å/s).

Results

To best appreciate the results described below, it is useful to first summarize the essential characteristics of the potential-controlled surface forces for the system under study. The interaction between the gold electrode and the mica becomes more attractive as the applied potential on the gold electrode is made more positive. This is because mica develops a negative surface potential of around −115mV in solution, independent of the applied potential on the gold electrode, caused by the dissociation of potassium ions from the surface.[14,18,19] The dependence of adhesion on applied potential is caused by an increased charge density at the gold surface. The extent of the attraction between gold and mica diminishes as the gold potential becomes less positive down to a point called the potential of zero force (PZF), which can be seen as the transition potential between attractive and repulsive interactions. The PZF occurs at a similar potential as the potential of zero charge (PZC).[10]

Figure 1 shows the basic geometry of the interacting surfaces as configured in the SFA. Motors can be used to position the base of the cantilever spring at any desired location. The spring deflects to balance the forces acting between the surfaces. Hence, the relative displacement between the surfaces can be altered by changing the surface forces solely through potential control. Note the similarity between the configuration in the SFA and that of an electrostatic actuator: both have two charged surfaces, one attached to a spring and the other that is rigidly mounted (as illustrated in Figure 1(d)). The main difference is that in our case, the DC potential applied to the gold electrode is independent of the surface potential of the mica surface (it is an asymmetric parallel-plate actuator). This allows repulsive and attractive interactions to be investigated. When the surfaces are out of contact, the electrostatic force is balanced by the cantilever force, while in contact a contact force caused by the elastic deformation (compliance) is introduced to the force balance.

Shaping Contact. Contact is conveniently created using the following scheme: First, the separation between the two surfaces is reduced to reach a gap of 10−100 nm using the microstepping motors. From this point on, the surfaces are never mechanically moved in or out of contact (i.e., the motors are no longer necessary to control surface separation or the applied load). Similar to the situation of a parallel plate actuator, the surface separation is governed by a balance between the surface forces (which are controlled via the applied potential) and the cantilever force. This means that, at all times, upon an incremental change in potential (with no additional mechanical input to the system), the spring will deflect until the balance is restored, following a path with slope equal to the spring constant. If the potential step renders the interaction more repulsive, then the surfaces will move apart and if the interaction becomes more attractive, the surfaces will move closer to contact.

In the case shown here, the two surfaces are first mechanically brought to close proximity (20 nm apart) under the influence of strong repulsive double layer interactions; the applied potential on the gold surface is −0.37 V (this situation is shown schematically in Figure 1b). The applied potential is then changed to a value (+0.39 V), whereupon the interaction between the surfaces is sufficiently attractive that the surfaces get into contact.

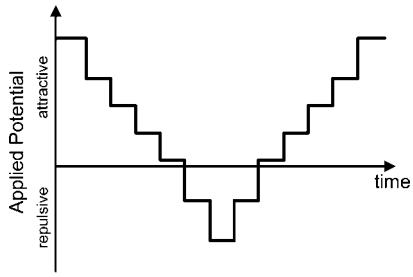

Figure 2. Potential cycling steps employed in the experiment described herein. Each potential step is maintained for 2 min, after which a picture of the fringes is taken with a CCD camera.

Having used a change in applied potential to make contact, we demonstrate how further changes in potential can be used to shape contact. In contact, the cantilever force is balanced by the surface force and the contact force (i.e., the elastic deformation). Figure 2 shows the input potential cycle employed. At each applied potential a CCD camera is used to obtain an intensity profile of interference fringes that geometrically correspond to a slice of the interacting surfaces, the intensity profile is then converted into surface separation using the multimatrix method.[20] (Note that surfaces in an SFA are in a cross-cylinder geometry, which is equivalent to that of a sphere and a plane). Figure 3a displays such a slice showing the surface separation vs lateral separation taken after the contact is made at an applied potential of 0.39 V. The apex of the curve (corresponding to the contact area) is flattened due to the deformation of the glue under the mica surfaces. The profiles observed in Figure 3 are parabolic due to the different scale of the x and y axes (microns vs nanometers). By fitting the profile with the equation of an undeformed sphere of the same radius as the radius of curvature, a deformation at contact of 2 nm is determined, and a contact area of $\sim$130 μm^2 is obtained.

Once contact is made, changing the applied potential allows us to control the deformation of the surfaces (without employing the motors). Figure 3b demonstrates this possibility by showing the change in contact area as the applied potential is switched between 0.39 V and 0.04 V. The contact area decreases when the applied potential is made less positive (when the potential is switched between 0.39 V to 0.04 V) due to the reduced attraction between the surfaces. As seen in Figure 3b, the contact area decreases by 75% upon a potential change. This process is fully reversible, as the contact area goes back to its initial value once the applied potential is returned to 0.39 V.

The incremental spring deflection between each potential step can be extracted from the fringe profiles by evaluating changes in gap displacement away from the contact region, at a separation for which the surface profile is undeformed (i.e., uninfluenced by local elastic deformation of the interacting substrates). Shown in Figure 4 is an enlargement of the region 30−40 μm laterally away from the point of closest approach. The interferometry employed in the SFA allows resolution of surface profiles with subnanometer resolution even 10 μm away from the contact area (and with micron resolution in the lateral direction). Here, very far from the point of closest approach, one can measure reversible changes in surface separation of a few nanometers solely caused by a variation in the applied potential. The total deflection can then be obtained by adding the original deflection (which is readily available from the force at the last position before the potential cycling). The total mechanical load on the system for each applied potential is obtained by multiplying the total deflection by the spring constant. The mechanical loads, in addition to the observed deflections, are given in Table 1. At each applied potential, the total deflection is evaluated at five different lateral separations taken between 30−80 μm away from the point of closest approach (i.e., for five points in the fringe profile). The average deflections and standard deviations reported in Table 1 are calculated from the five measurements. No systematic variation in deflection was observed within the small window of lateral separations used for the calculation. The total deflection is positive at all potentials because initially when the gold electrode is at −0.37 V the surfaces are separated by 20 nm while the spring deflection is 76 nm, therefore as the potential is changed to 0.39 V, the surfaces reach contact without passing through zero deflection (i.e., it is spring-loaded). If it were possible to make the potential significantly more positive while avoiding electrolysis, then a zero deflection value could be obtained. From the values listed in Table 1, one can readily see that the spring force is compressive at each potential. This means that in contact the attractive force and the compressed spring compete against a repulsive contact force (this also implies that the surfaces did not reach a primary minimum during the potential cycling). At all potentials, the load exerted by the spring on the surface is very small ($\sim$7 μN) compared to the surface forces and compliance. Therefore we are very close to JKR[21] limit of no applied load for which the compliance directly balances the surface forces.

In contact (coincidentally for the data at positive potentials in Table 1), the deformation is mainly caused by the change in

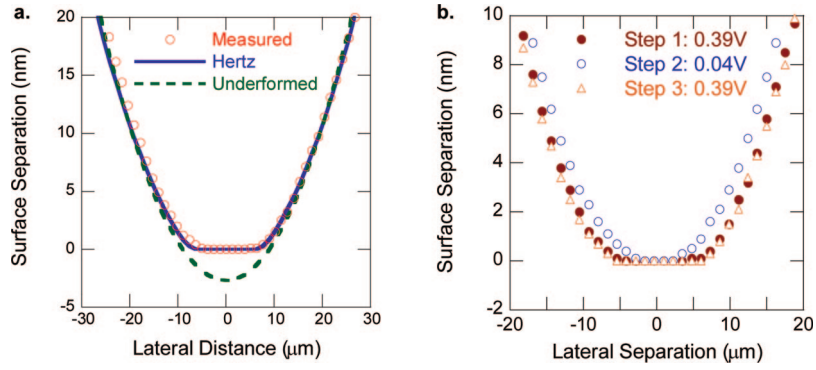

Figure 3. (a) Surface profile taken after the jump in contact at an applied potential of 0.39V (vs Ag/AgCl (3M)). The data points show the profile taken using the CCD camera and the solid line represents the calculated profile of an undeformed sphere with the same radius of curvature (1.5 cm). The deformation at the contact is 2 nm and the contact area is $\sim$130 μm^2. The dashed line represents the profile calculated for a Hertzian contact. (b) Surface profiles taken at three potential steps. The contact area is reduced by 75% when the applied potential goes from 0.39V to 0.04 V. The surfaces go back to contact and recover with the same area when the potential returns to 0.39 V.

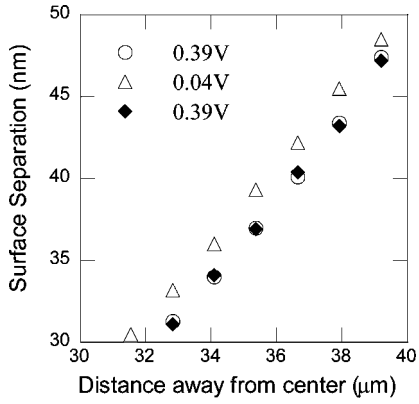

Figure 4. Selected region of the surface profile of Figure 3b taken 30−40 μm away from the contact region. The displacement caused by the change in applied potential is visible as well as the reversibility of the approach.

Table 1. Measured Deflection and Load for the Different Potential Steps[a]

potential (V)	incremental deflection (nm)	total deflection (nm)	applied load (μN/m)	contact radius (μm)
0.39	0	53.9	496	8.9
0.24	0.4 ± 0.2	54.3	500	6.4
0.14	0.2 ± 0.2	54.5	501	5.0
0.04	1.2 ± 0.1	55.7	512	4.5
−0.07	1.0 ± 0.1	56.7	522	0.6
−0.22	17.5 ± 0.4	74.2	683	N/A
−0.37	1.8 ± 0.1	76.0	699	N/A
−0.22	−2.1 ± 0.1	73.9	680	N/A
−0.07	−16.8 ± 0.3	57.1	525	N/A
0.04	−1.0 ± 0.1	56.1	516	2.5
0.14	−0.9 ± 0.2	55.2	508	3.8
0.24	−0.6 ± 0.2	54.6	502	5.7
0.39	−0.7 ± 0.2	53.9	496	6.4

[a] The initial total deflection (at 0.39V) is obtained from the force measured prior to the first potential step. Subsequent deflections are obtained from the fringe position away from the contact area (average of 5 points between 30 and 80 μm away from the contact area). The applied load is calculated from the deflection and the spring constant.

surface energy of the gold electrode with applied potential. This can be shown by comparing the change in load we observe with the change in contact radius. For surfaces in intimate contact, the force balance must include a contact force due to the compliance of the materials (i.e., the forces at play are the spring force, contact force, and the surface forces). In the simple case of Hertzian contact, the load has to *increase* for the contact radius to increase. In our experiments (see Figure 3b, and Table 1), we observe a *decrease* in the applied load for applied potentials leading to larger contact radius. Therefore, the change in radius has to come directly from a change in surface energy at the gold/mica contact. Depending on the desired technological application, the extent of deformation could be tuned by changing the compliance or the spring constant.

Electrostatic Actuation. The approach described here can be extended to the control of surface separation when the interacting surfaces are not in intimate contact. This capability is shown in Figure 5a, where we show that the surfaces can be moved out of contact to ∼20 nm separation and back by externally changing the charge on the gold surface via changes in applied potential. We now illustrate how the SFA could be employed to extract voltage-displacement relationships within nanoscale gaps.

We can extract directly and accurately the total deflection at each applied potential, and shown in Figure 5b is the measured relationship between the total spring deflection and the applied potential. If we focus on the region of negative applied potentials, then we observe that all three measurements shown in Figure 5b were made with the surfaces out of contact (the separation for an applied potential of −0.06 V is 0.5 nm, well within the resolution of the SFA). Salt solutions are electrically conducting, which prevents the large displacement required for the operation of DC electrostatic actuator at the micron-scale. At the nanoscale, displacement is achievable because the Debye length is on the same order of the gap between the plates (double layer overlap is required for displacement). As seen in Figure 5b, the relationship between voltage and displacement within the out of contact region is strongly nonlinear, possibly because the potential distribution between the two surfaces is also nonlinear and follows the Poisson−Boltzmann equation. For this observation, it is not critical to distinguish if the point at −0.06 V is slightly out of contact or if it has just reached contact, as in the latter case an incrementally more negative potential would keep the surfaces apart resulting in an even steeper slope between the second and third points. The nonlinear nature of double-layer interactions is also observed when the force at fixed separation is plotted as a function of applied potential. These force-voltage relationships are shown in the literature as a means to determine the potential of zero force (PZF).[10−12,14,15,22,23] In practice, the PZF is obtained by first measuring a multitude of force curves at different potentials and then mining the raw data. The approach described here to characterize electrostatic actuation in small gaps is more rapid and has the advantage that the deflection-voltage relationship can be extracted directly in one set of measurements.

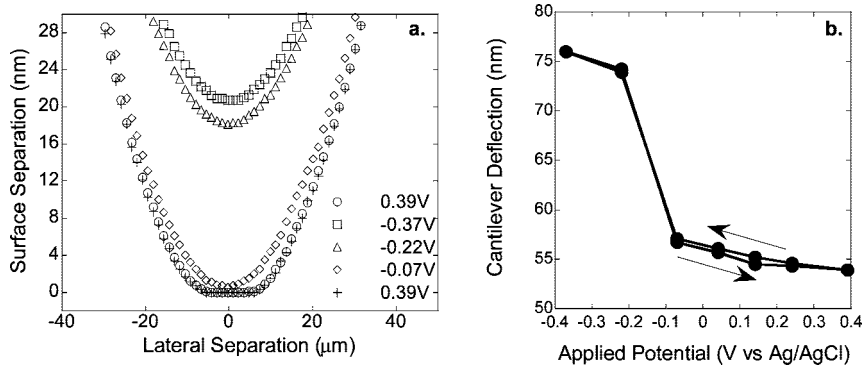

Figure 5. (a) Series of surface profiles taken as the potential is brought to negative values such that the surfaces move out of contact. The surfaces come back to the same original position when the potential is brought back to its initial potential. (b) Total cantilever deflection as a function of applied potential. The calculated values for the deflection are extracted from the series of surface profiles shown in Figure 5. Note that the data points at negative applied potential are (coincidentally) out of contact.

As an aside, the lack of hysteresis in these measurements is somewhat surprising, but not uncommon.[24] A strong primary minimum caused by Van der Waals interactions could prevent the surfaces from being moved in and out contact in a completely reversible fashion, as we indeed observe. It is possible that surface roughness and contamination prevent van der Waals forces from taking over at contact. We note that measurable van der Waals forces were present, however, when the gold and mica surfaces were brought into contact in air at the beginning of the experiment and we did not observe any change (within the 0.3 nm resolution) in the contact position when the surfaces were brought together in solution.

The fine level of control over contact area and surface separation achievable with the electrochemical SFA opens the door to study electrostatic actuation in nanoscale gaps and to design schemes employing such electrocapillary actuation between two solid surfaces as the basis for a switch or gate. Furthermore, this demonstrates that the electrochemical SFA can be effectively used to test new methods of surface-driven actuation. To enable and control the displacement of surfaces separated by tens of nanometers, reversible variations in the overlap of double layers can be used to make or break contact. As a limitation, it is important to note that the onset of double layer overlap depends strongly on the salt concentration in solution.[25] From our prior characterization of double layer forces as a function of applied potential for this system,[14−16] it is believed that the control of displacement in salt solutions of up to 100 mM (which corresponds to a Debye length of 0.96 nm) is feasible using dynamic control of surface energy. For higher concentrations, an AC actuation could potentially be used and the electrochemical SFA could be employed to determine the deflection-voltage relationship.

Conclusions

In this work, we have shown how the electrochemical SFA can be employed as a model electrostatic actuator operating at the nanoscale. We described how a change in surface charge at an electrode surface can shape contact and actively change surface separation. Variation in the contact area is observed for different applied potentials without moving the motors or otherwise changing the applied load. Changing the potential while the interacting surfaces are in contact is equivalent to changing the surface energy and we can monitor the corresponding contact area while doing so. We demonstrated that we are able to extract voltage-deflection relations for surface separation less than 100 nm. In addition, controlling double layer forces could be employed as a mode of actuation, as long as the separation between the two surfaces is within the double layer overlap.

Acknowledgment

With great pride and pleasure, this paper is dedicated to John Anderson—friend, mentor, and soul of the magnificent Quinn academic family, which adopted one of us (T.K.V.) early in her career and showed her the way. This work was funded through National Science Foundation via the Materials Research Science and Engineering program Grant DMR 0213706.

Literature Cited

(1) Grayson, A. C. R.; Shawgo, R. S.; Johnson, A. M.; Flynn, N. T.; Li, Y. W.; Cima, M. J.; Langer, R. A BioMEMS review: MEMS technology for physiologically integrated devices. *Proc. IEEE* **2004**, *92*, 6–21.

(2) Parker, E. E.; Ashurst, W. R.; Carraro, C.; Maboudian, R. Adhesion characteristics of MEMS in microfluidic environments. *J. Microelectromech. Syst.* **2005**, *14*, 947–953.

(3) Sounart, T. L.; Michalske, T. A.; Zavadil, K. R. Frequency-dependent electrostatic actuation in microfluidic MEMS. *J. Microelectrochem. Syst.* **2005**, *14*, 125–133.

(4) Sniegowski, J. J.; Garcia, E. J. In Microfabricated actuators and their application to optics, *Miniaturized Systems With Micro-Optics and Micromechanics*; Motamedi, M. E., Beiser, L. Eds.; SPIE: San Jose, CA, 1995; pp 46−64

(5) Nemirovsky, Y.; Bochobza-Degani, O. A methodology and model for the pull-in parameters of electrostatic actuators. *J. Microelectromech. Syst.* **2001**, *10*, 601–615.

(6) Bochobza-Degani, O.; Nemirovsky, Y. Modeling the pull-in parameters of electrostatic actuators with a novel lumped two degrees of freedom pull-in model. *Sens. Actuators, A* **2002**, *9*, 7–8.

(7) Bochobza-Degani, O.; Socher, E.; Nemirovsky, Y. On the effect of residual charges on the pull-in parameters of electrostatic actuators. *Sens. Actuators, A* **2002**, *97* (8), 563–568.

(8) Rollier, A. S.; Legrand, B.; Collard, D.; Buchaillot, L. The stability and pull-in voltage of electrostatic parallel-plate actuators in liquid solutions. *J. Micromech. Microeng.* **2006**, *16*, 794–801.

(9) Boyd, J. G.; Kim, D. Nanoscale electrostatic actuators in liquid electrolytes. *J. Colloid Interface Sci.* **2006**, *301*, 542–548.

(10) Hillier, A. C.; Kim, S.; Bard, A. J. Measurement of Double-Layer Forces at the Electrode/Electrolyte Interface Using the Atomic Force Microscope: Potential and anion Dependant Interactions. *J. Phys. Chem.* **1996**, *100*, 18808.

(11) Raiteri, R.; Grattarola, M.; Butt, H.-J. Measuring Electrostatic Double-Layer Forces at High Surface Potentials with the Atomic Force Microscope. *J. Phys. Chem.* **1996**, *100*, 16700–16705.

(12) Raiteri, R.; Preuss, M.; Grattarola, M.; Butt, H.-J. Preliminary results on the electrostatic double-layer force between two surfaces with high surface potentials. *Colloid Surface A* **1998**, *136*, 191–197.

(13) Wang, J.; Bard, A. J. Direct Atomic Force Microscopic Determination of Surface Charge at the Gold/Electrolyte Interface- The inadequacy of Classical GCS theory in Describing the Double-Layer Charge Distribution. *J. Phys. Chem. B* **2001**, *105*, 5217–5222.

(14) Frechette, J.; Vanderlick, T. K. Impact of Pyridine Adsorption on the Interactions between a Gold Electrode and a Mica Surface. *J. Phys. Chem. B* **2005**, *109*, 4007–4013.

(15) Frechette, J.; Vanderlick, T. K. Electrocapillary at contact: potential dependent adhesion between a gold electrode and a mica surface. *Langmuir* **2005**, *21*, 985.

(16) Frechette, J.; Vanderlick, T. K. Double layer forces over large potential ranges as measured in an electrochemical surface forces apparatus. *Langmuir* **2001**, *17*, 7620–7627.

(17) Ives D. J. G.; Janz, G. J. *Reference Electrodes, Theory and Practice*; Academic Press: New York; 1961, p 651.

(18) Pashley, R. M. DLVO and Hydration forces between surfaces in Li+, Na+, K+, and Cs+ electrolyte solutions: A correalation of doublelayer and hydration forces with surface cation exchange properties. *J. Colloid Interface Sci.* **1981**, *83*, 531–546.

(19) Shubin, V. E.; Kekicheff, P. Electrical Double Layer Structure revisited via a surface force apparatus: Mica interfaces in lithium nitrate solutions. *J. Colloid Interface Sci.* **1993**, *155*, 108–123.

(20) Levins, J. M.; Vanderlick, T. K. Extended Spectral analysis of multiple beam interferometry: a technique to study metallic films in the surface forces apparatus. **1994**, *10*, 2389–2394.

(21) Johnson, K. L.; Kendall, K.; Roberts, A. D. Surface Energy and Contact of Elastic Solids. *Proc. R. Soc. London, A* **1971**, *324*, 301–&.

(22) Campbell, S. D.; Hilller, A. C. Nanometer-scale probing of potential-dependent electrostatic forces, adhesion, and interfacial friction at the electrode/electrolyte interface. *Langmuir* **1999**, *15*, 891–899.

(23) Wang, J.; Feldberg, S. W.; Bard, A. J. Measurement of double-layer forces at the polymer film/electrolyte interfaces using atomic force microscopy: concentration and potential-dependent interactions. *J. Phys. Chem. B* **2002**, *106*, 10440–10446.

(24) Barten, D.; Kleijn, J. M.; Duval, J.; von Leeuwen, H. P.; Lyklema, J.; Stuart, M. A. C. Double layer of a gold electrode probed by AFM force measurements. *Langmuir* **2003**, *19*, 1133–1139.

(25) Russel, W. B.; Saville, D. A.; Schowalter, W. R. *Colloidal Dispersions*; Cambridge University Press:New York; 1989, p 525.

Received for review May 6, 2008
Revised manuscript received July 8, 2008
Accepted July 9, 2008

IE800734Y